Title:

Reciprocal cybrids reveal how organellar genomes affect plant phenotypes

Key words: Arabidopsis, Chloroplast, Cytonuclear interaction, Epistasis, Mitochondrion, Plant growth, Photosynthesis

Authors:

Pádraic J. Flood[1,2,3†*], Tom P.J.M. Theeuwen[1†*], Korbinian Schneeberger[3], Paul Keizer[4], Willem Kruijer[4], Edouard Severing[3], Evangelos Kouklas[1], Jos A. Hageman[4], Frank F.M. Becker[1], Sabine K. Schnabel[4], Leo Willems[5], Wilco Ligterink[5], Jeroen van Arkel[6], Roland Mumm[6], José M. Gualberto[7], Linda Savage[8], David M. Kramer[8], Joost J.B. Keurentjes[1], Fred van Eeuwijk[4], Maarten Koornneef[1,3], Jeremy Harbinson[2], Mark G.M. Aarts[1] & Erik Wijnker[1*]

Affiliations:

[1] Laboratory of Genetics, Wageningen University & Research, Wageningen, The Netherlands.

[2] Horticulture and Product Physiology, Wageningen University & Research, Wageningen, The Netherlands.

[3] Department of Plant Developmental Biology, Max Planck Institute for Plant Breeding Research, Cologne, Germany.

[4] Biometris, Wageningen University & Research, Wageningen, The Netherlands.

[5] Laboratory of Plant Physiology, Wageningen University & Research, Wageningen, The Netherlands.

[6] Bioscience, Wageningen University & Research, Wageningen, The Netherlands

[7] Institut de Biologie Moléculaire des Plantes, CNRS, Université de Strasbourg, Strasbourg, France.

[8] MSU-DOE Plant Research Lab, Michigan State University, East Lansing, USA

[†] These authors contributed equally to this work

* Correspondence to:

P.J. Flood - flood@mpipz.mpg.de

T.P.J.M. Theeuwen - tom.theeuwen@wur.nl

E. Wijnker - erik.wijnker@wur.nl

Abstract: Assessing the impact of variation in chloroplast and mitochondrial DNA (the plasmotype) on plant phenotypes is challenging due to the difficulty in separating their effect from nuclear derived variation (the nucleotype). By using haploid inducer lines as plasmotype donors we employed an efficient and precise method to generate a panel comprising all possible cytonuclear combinations (cybrids) of seven *Arabidopsis thaliana* accessions. We screened these lines for different plant performance parameters, yielding 1008 phenotypes. Plasmotype-induced phenotypic variation is highly epistatic with nuclear variation and can be of large effect, i.e. increasing plant biomass by as much as 23%. Four times as much variation is explained by cytonuclear interactions as opposed to an additive effect of the plasmotype. This quick and precise method allows the detection of cytonuclear interactions, and may allow improving plant performance through efficient screening for favourable nucleus-organelle combinations.

Main Text: Mitochondria and chloroplasts play essential roles in plant respiration, photosynthesis and primary metabolism. Their genomes contain genes essential for these processes, but their functioning requires tight coordination with the nucleus since the majority of organellar proteins are encoded in the nucleus. This dependence, together with signaling pathways that modulate nuclear and organellar gene expression (Kleine and Leister, 2016), can cause complex interactions and non-additive, non-linear effects (epistasis). The phenotypic consequences of epistasis can be detected when a plasmotype causes phenotypic effects in combination with some, but not all nuclear backgrounds. Indeed, recent studies suggest that cytonuclear epistasis is not uncommon (Joseph et al., 2013; Joseph et al., 2013; Tang et al., 2014; Roux et al., 2016). In contrast to simpler predictable additive effects, in which a plasmotype causes consistent changes with any nucleus it is combined with, epistasis is unpredictable when its underlying causes are unknown.

Organellar sequence variation is relevant from an agricultural as well as evolutionary perspective (Levings, 1990; Bock et al., 2014; Dobler et al., 2014), but to understand, or utilize it, it is necessary to assess its additive and epistatic components. To do so, and to study plasmotypic variation, dedicated methods have been developed to separate nuclear from mitochondrial and chloroplastic effects. Reciprocal-cross designs, where nucleotypes segregate in different plasmotypic backgrounds, revealed plasmotype-specific quantitative trait loci (Joseph et al., 2013; Tang et al., 2014), but in these populations the variation from just two plasmotypes is assessed. A wider range of

plasmotypes can be studied using backcross designs where plasmotypes are introgressed into different nuclear backgrounds (Miclaus et al., 2016; Roux et al., 2016), but backcross approaches are lengthy and any undetected nuclear introgressions may confound the results.

To precisely and rapidly address the contribution of organellar variation to plant phenotypes, we explored the use of a haploid inducer line available in Arabidopsis (*GFP-tailswap*) (Ravi and Chan, 2010). This line expresses a GFP-tagged CENTROMERE HISTONE 3 protein in a *cenh3/htr12* mutant background. When pollinated with a wild-type plant, the *GFP-tailswap* nuclear genome is lost from the zygote through uniparental genome elimination, generating haploid offspring (Fig. 1). Since the plasmotype of the resulting offspring is maternal in origin, the haploid offspring are cybrids, combining a paternal nucleus with the maternal *GFP-tailswap* mitochondria and chloroplasts. These haploid plants produce diploid (doubled haploid) offspring following genome duplication or restitutional meiosis (Ravi and Chan, 2010). Using the *GFP-tailswap* it is possible to generate cybrids in two generations, and in just four generations for all possible nucleotype-plasmotype combinations (Fig. 1A and 1B) (Kindiger and Hamann, 1993; Ravi and Chan, 2010; Ravi et al., 2014). We set out to test the use of this approach to investigate how plasmotypic variation affects plant phenotypes and to what extent this variation manifests itself as additive variation or as cytonuclear epistasis.

Seven different Arabidopsis accessions were selected: six that represent a snapshot of natural variation, and one accession (Ely) that has a large-effect mutation in the chloroplast-encoded *PsbA* gene which results in reduced photosystem II efficiency and a constitutively oxidized plastoquinone pool under light-limited conditions (El-Lithy et al., 2005; Flood et al., 2014). The Ely accession was included to evaluate the consequence of a strong plasmotype effect in our test-panel. We first generated haploid inducers for all seven plasmotypes and then used each inducer to generate cybrid offspring for all seven nucleotypes (Fig. 1C). Wild-type nucleotype-plasmotype combinations were also regenerated in this way (hereafter referred to as self-cybrids) to later compare these with their wild-type progenitors. Nuclear, mitochondrial and chloroplastic genotypes of cybrids were verified by whole genome sequencing, confirming that the cybrid genotypes were as expected and there were no nuclear introgressions (Supplementary Fig. 1 and 2). SNP data were used to generate neighbor joining trees for the nuclear, mitochondrial and chloroplastic genomes (Supplementary Fig. 3). The nucleotypes are approximately equidistant whilst the mitochondrial and chloroplastic genomes showed larger variance in relatedness, with Sha being most diverged.

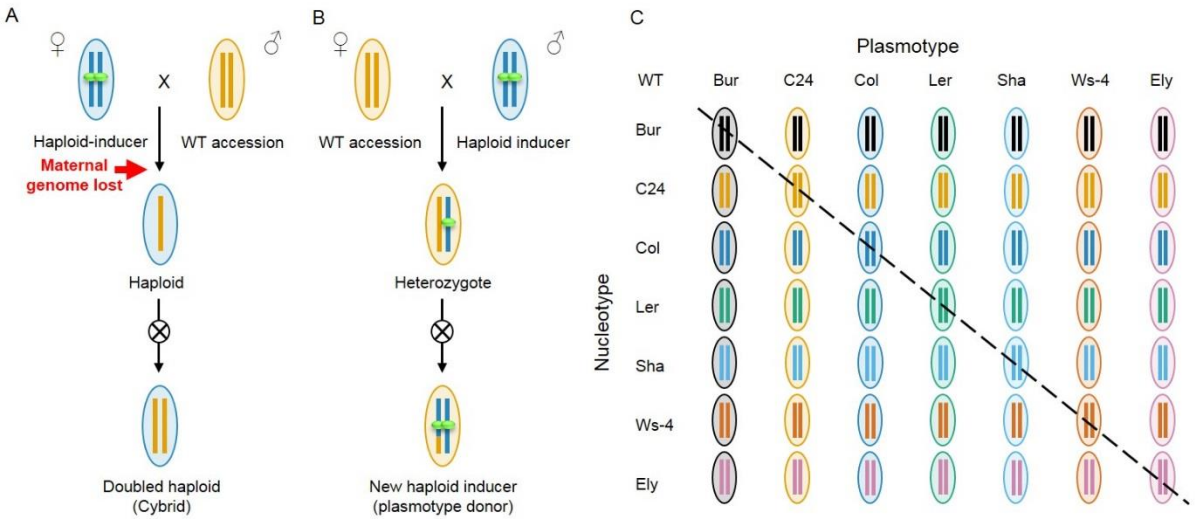

Figure 1. Generation of a cybrid test panel. A) Haploid-inducers (HI) can function as plasmotype donors when used as a female parent. In this case, uniparental genome elimination (red arrow) leads to a haploid offspring plant with the nucleotype of the wild-type (WT) male parent, but the plasmotype of the HI mother. B) Generation of a HI line with a new plasmotype. A cross of a wild type (female) with a HI (male) results in a hybrid F1. A diploid F1 is selected in which no genome elimination has occurred. Self-fertilization generates an F2 population in the plasmotype of the wild-type mother. From this an F2 is selected that is homozygous for the *cenh3/htr12* mutation, but carries the *GFP-tailswap*. This F2 plant is a new HI line and can serve as plasmotype donor when used as female in crosses. Vertical bars represent the nucleotype, and the ovals represent the plasmotype. HI centromeres are indicated in green (signifying GFP-tagged CENH3/HTR12 proteins as encoded by the *GFP-tailswap* construct) that cause uniparental genome-elimination. C) Full diallel of all nuclear-plasmotype combinations. The diagonal line highlights the wild-type (WT) nucleotype-plasmotype combinations that were generated by crossing wild-type plants to plasmotype donors with the identical plasmotype. These wild-type nucleotype-plasmotype combinations are referred to as “self-cybrids”.

We phenotyped the cybrid panel for absolute and relative growth rate, biomass accumulation, epinastic leaf movement, photosystem II efficiency (φ_{PSII}), non-photochemical quenching (NPQ) including rapidly relaxing (q_E) and slowly relaxing (q_I) components of NPQ, a reflectance-based estimate of chlorophyll, flowering time and germination under constant environmental conditions. In addition, to reflect more natural conditions we screened the panel under fluctuating light for all photosynthesis-related traits, and assayed germination rates under osmotic stress and after a controlled deterioration treatment. We also measured 41 primary metabolites using gas chromatography coupled with time-of-flight mass spectrometry (GC-ToF-MS). A total of 1008 phenotypes were scored, counting individual metabolite concentrations and single time points in time series as separate phenotypes (Supplementary Data 1). Phenotypes with a broad sense heritability (H^2) of less than 5% were removed from analysis, leaving a total of 906 phenotypes. To avoid overrepresentation of time series and highly correlated traits, we selected a subset of 34 representative phenotypes (Supplementary Table 1) comprising 22 from constant growth conditions and 12 from fluctuating environmental conditions which we used for further analysis. The analysis using the full set of 906 phenotypes is included in the supplemental material.

Comparison of self-cybrids with their genetically identical wild-type progenitors did not reveal any phenotypic differences (Supplementary Table 1) from which we infer that cybridization through uniparental genome elimination is a robust method to generate cybrids. To determine the relative contributions of nucleotype, plasmotype, and their interaction, to the observed phenotypic variation we estimated the fraction of the broad sense heritability (H^2) explained by each. Across the entire panel the average contribution to H^2 of nucleotype, plasmotype and nucleotype-plasmotype interaction was 58.7%, 34.4% and 6.8% respectively (Supplementary Table 2 and 3; Supplementary Data 1). Most of the variation in the plasmotype was caused by the Ely plasmotype, probably arising from the mutation in its *PsbA* gene. When this plasmotype was excluded from the analysis, the nucleotype, plasmotype and their interaction account for 95.2%, 1.0% and 3.8% of the genetic variation (Fig. 2). So, while nucleotype-derived additive variation is the main genetic determinant of the cybrid phenotype, variation caused by cytonuclear interactions (epistasis) is almost four times larger than the additive effect of the plasmotype (p=0.000095).

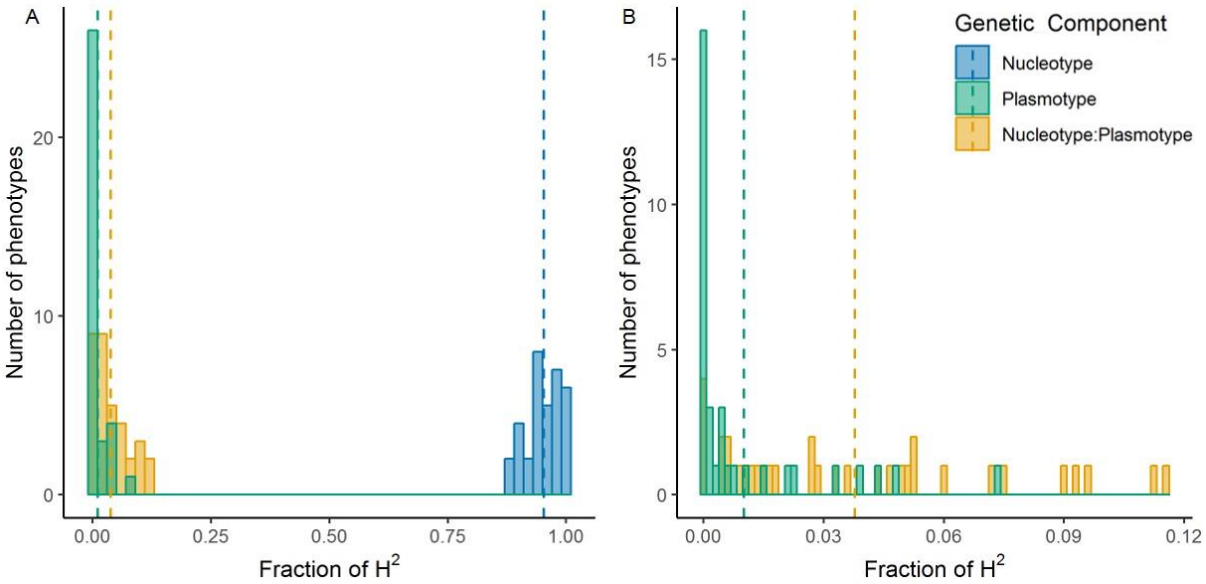

Figure 2. The nucleotype-plasmotype interaction explains more variation than the plasmotype. Distribution of the fraction of broad sense heritability (H^2) for the three genetic components (nucleotype, plasmotype and the nucleotype-plasmotype interaction). Data given for 34 representative phenotypes. Dashed lines indicate the average H^2 for each component; B) is a subset of A). See Supplementary Fig. 5 for plots on the complete set of 906 phenotypes.

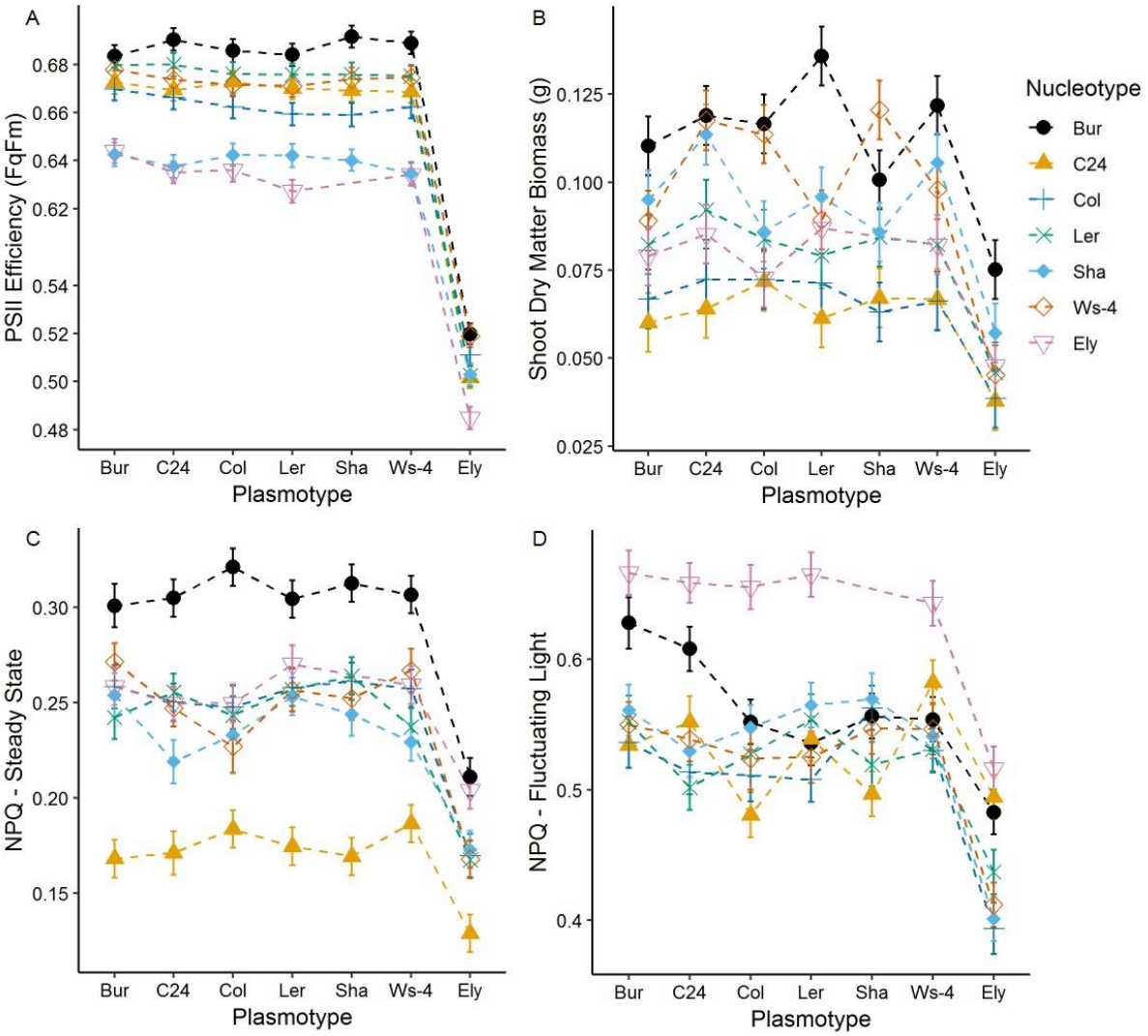

Figure 3. Plasmotype changes result in cytonuclear epistasis, except in the case of cybrids with the Ely plasmotype which show additive effects. Phenotypes of the 48 examined cybrid lines for A) PSII efficiency (φ_{PSII}) for electron transport at 13.4 days after sowing (DAS) (n=24) B) Shoot dry matter biomass (g) at 30 DAS (n=12) C) NPQ at 17.96h into the measurement during constant environmental conditions of 200 µmol m^{-2} s^{-1} (n=4) D) NPQ at 66.79h into the measurement on the same plants as in C), measured at 496 µmol m^{-2} s^{-1} right after 1000 µmol m^{-2} s^{-1} (n=4). Error bars represent the standard error of the mean.

Though the total explained variance due to the cytonuclear interaction is only 3.8% on average, this interaction can be large for specific phenotypes or in specific cybrids. For example, as much as 7.2% of the total genetic variation for rosette dry weight (biomass) is explained by cytonuclear interactions. In the cybrid with a Bur nucleotype and L*er* plasmotype (Bur^{Ler}) this amounts to an increase of 23% in shoot biomass when compared to the wild-type Bur^{Bur} cytonuclear combination (p=0.008). In another example, 9.7% of the total genetic variance for NPQ under fluctuating light is explained by cytonuclear interactions, with Bur^{Ler} showing a 17.2% reduction as compared to Bur^{Bur}. This effect is only triggered under more challenging conditions, since this difference in NPQ does not occur under continuous light (Fig. 3C and 3D).

Considering that most of the observed phenotypic changes result from epistasis, and these are unique to specific nucleotype-plasmotype combinations, we sought to assess whether there are general patterns in how specific nucleotypes and plasmotypes interact. We therefore compared wild-type nucleotype-plasmotype combinations with all their iso-nuclear cybrid lines (Table 1). The Bur nucleotype shows significant differences for 28 phenotypes when combined with non-native plasmotypes (excluding the Ely plasmotype) (Table 1). In contrast, Col and Sha show just one and three, respectively, thus within the scope of this panel their nucleotypes are most tolerant of genetic variation in the plasmotype. Conversely, cybrids with the Bur plasmotype show just three significantly altered phenotypes as compared to 21 in cybrids that have a Sha plasmotype. Sha, which is the most genetically distant plasmotype (Supplementary Fig. 3) in our panel, causes most significant phenotypic changes in combination with other nucleotypes. Thus, plasmotypes and nucleotypes differ in their likelihood of producing significant cytonuclear interactions, with genetic distance possibly influencing the extent of epistasis.

Table 1. Plasmotype changes cause significant changes in plant phenotypes. Significant changes in plant phenotypes between wild-type nucleotype-plasmotype combinations (self-cybrids) and cybrids with different plasmotypes for 34 selected phenotypes (Supplementary data 2 for underlying phenotypes). Rows indicate the number of significant effects when comparing self-cybrids to cybrids with identical nucleotype but non-native plasmotype. Columns indicate the changes when plasmotype is kept constant. Note that the Ely^{Ely} self-cybrid shows many significant changes compared with Ely^{XXX} cybrids (bottom row) and that the XXX^{Ely} cybrids show many significant changes compared with XXX^{XXX} self-cybrids (last column), which is due to the large-effect mutation in the chloroplast-encoded PsbA gene of the Ely plasmotype. Posthoc test done with Dunnet, α = 0.05. nd = not determined. For underlying p-values, see Supplementary data 2. Yellow cells indicate low numbers of significant changes; blue cells show higher number of significant changes.

# of significant phenotypes 0 11 22		Plasmotype						
		XXX^{Bur}	XXX^{C24}	XXX^{Col}	XXX^{Ler}	XXX^{Sha}	XXX^{Ws-4}	XXX^{Ely}
wildtype nucleotype-plasmotype combination	Bur^{Bur}		1	6	7	11	3	19
	$C24^{C24}$	0		3	0	3	0	17
	Col^{Col}	1	0		0	0	0	20
	Ler^{Ler}	0	0	1		3	5	22
	Sha^{Sha}	2	1	0	0		0	15
	$Ws\text{-}4^{Ws-4}$	0	2	0	0	4		21
	Ely^{Ely}	17	21	19	17	nd	14	

The Ely plasmotype is unique in our panel because it contributes strong additive effects due to the lower quantum yield of electron transport caused by the *PsbA* mutation in its chloroplast. The *PsbA* mutation was selected for in response to the use of triazine herbicides along English railways from the 1960s onwards (Flood et al., 2016). Cybrids with the Ely plasmotype all have a lower PSII efficiency (Fig. 3A) and lower values for other photosynthesis related traits i.e. NPQ, q_E and chlorophyll content (Fig. 3C and Supplementary Fig. 5). The reduced PSII efficiency (φ_{PSII}) is likely to be responsible for the concomitant reductions in biomass (Fig. 3B), growth rate and seed size (Supplementary Data 2). There is also a reduction in serine and glycine content of cybrids with Ely plasmotye, which is often associated with lower photorespiration and may result from reduced carbon fixation (Somerville and Ogren, 1980). In the presence of the Ely plasmotype we detected additive changes in 30 out of 34 selected phenotypes and changes in the concentrations of 28 out of 41 measured primary metabolites (Supplementary Data 2). Interestingly, the Ely nucleus shows a 15% increase in NPQ under fluctuating light conditions as compared to the average of all other nuclei in our panel (Fig. 3D). It is tempting to hypothesize that this results from a compensatory mutation to balance the 21% loss of NPQ conferred by the Ely plasmotype. Although, whether the high NPQ in the Ely nucleus then results from genuine co-adaptation, or whether it was a pre-existing nuclear trait that may have facilitated the selection for atrazine resistant chloroplasts we cannot say with our current dataset.

We contrasted the transcriptome of the Bur, L*er* and Ely accessions and their six reciprocal cybrids (Supplementary Data 3) to better understand the Ely additive effect and determine which transcriptional pathways changed in reciprocal cybrids between Bur and L*er* for which we observed significant phenotypes for the Bur^{Ler} cybrid line (see table 1). Replacing the native plasmotype with the Ely plasmotype in L*er* and Bur changes the expression of 726 and 2230 of nuclear encoded genes. Unsurprisingly these genes are enriched for the GO term “photosynthesis” (GO:0006091)(Supplementary Data 3). Across all three nucleotypes only 23 genes are significantly differently expressed when either the Bur or L*er* plasmotype is replaced by Ely. Only one of these 23 genes, the pathogen response induced *β-1,3-GLUCANASE 3* (*BG3*, AT3G57240), is always upregulated when the Ely plasmotype is present (Supplementary Table 6). β-1,3-Glucanases act in the degradation of 1,3-β-D-glucosidic bonds which are frequently found in cell walls of many fungi, and in callose, a plant polysaccharide consisting mainly of β-1,3-glucans (Chen and Kim, 2009). Callose degradation can improve cell-to-cell trafficking of nutrients and signaling molecules through opening of

plasmodesmata, although so far, *BG3* has not been implicated in this (Zavaliev et al., 2013). The other 22 genes have different directions of response depending on the nuclear background. For example expression of *LUTEIN DEFICIENT 5* (*CYP97A3*), which encodes a heme-containing cytochrome P450 involved in the biosynthesis of xanthophylls and important in NPQ, is downregulated in the Bur and Ely nucleotypes while upregulated in the L*er* nucleotype. Thus, despite its additive effect on higher order phenotypes, the Ely plasmotype causes almost exclusively unique transcriptional changes in each nuclear background, highlighting that at the transcriptional level the Ely plasmotype effect is epistatic.

In the case of changing the Bur plasmotype for that of L*er* we detected no significant additive effects for any of the higher order phenotypes. Nonetheless, in the Bur nucleotype background, 820 nuclear genes were differentially expressed between Bur^{Bur} and Bur^{Ler} (Supplementary Fig. 6). Of these genes, 13 were classified under the GO term “glutathione transferase activity” (GO:0004364) and 8 under “glutamate receptor activity” (GO:0008066). Glutathione transferases (GSTs) have evolved to perform a range of functional roles, amongst which they have been implicated in acclimation to high light (Lv et al., 2015). Glutamate receptor-like proteins remain largely undescribed, but are linked to non-selective cation channels involved in metabolic and defense signaling mechanisms (Forde and Roberts, 2014; Toyota et al., 2018; Nguyen et al. 2018). The epistatic nature of cytonuclear interactions implies that these transcriptional changes (and the accompanying phenotypic differences, including the 23% difference in plant biomass) can only be observed and understood within the context of the Bur nucleus. In the L*er* nucleotype, the same Bur to L*er* plasmotype change affects gene expression of only three genes, and does not cause any significant change in higher order plant phenotypes (Table 1).

Our experiments have shown that a clean, systematic exploration of plasmotype variation in a plant species is feasible. The development of inducer lines for crop species would allow elite nucleotypes to be brought into new plasmotypic backgrounds to explore plamotype-nucleotype interactions and ultimately to optimize crop performance. Our data indicate that substantial gains in plant productivity can be made. We detected increases of as much as 23% for plant biomass, and a difference of 17.2% in NPQ under fluctuating light, which is increasingly recognized as important for plant productivity (Kromdijk et al., 2016). Exploring the potential of plasmotypic variation via the use of inducer lines is promising both for plant breeding and for understanding the ecological role such variation plays in plant adaptation (Bock et al., 2014; Dobler et al., 2014).

Author contributions: P.J.F. and E.W. conceived and designed the study. T.P.J.M.T. designed and performed the statistical analysis with help from P.J.F., W.K. and F.v.E.. P.J.F., T.P.J.M.T., E.K., F.F.M.B., L.W., J.v.A., J.M.G., and L.S. performed experiments. P.J.F., T.P.J.M.T., K.S., P.K., E.S., J.A.H., S.K.S., W.L., R.M., F.v.E. and E.W. analysed data. D.M.K., J.J.B.K., M.K., J.H. and M.G.M.A. contributed to the interpretation of results. P.J.F., T.P.J.M.T. and E.W. wrote the paper with significant contributions from M.K., J.H. and M.G.M.A. All authors read and approved the final manuscript.

Acknowledgements: Hetty Blankestijn, Jose van de Belt, Daniel Oberste-Lehn, Elio Schijlen, Corrie Hanhart, and Joris ter Riele (all Wageningen University & Research) are acknowledged for help with experiments, Jonas Klasen (Max Planck Institute for Plant Breeding Research) for statistical advice, and Duur Aanen (Wageningen University & Research) for helpful discussions.

Data availability: Sequencing and transcriptome data will be available in the European Nucleotide Archive with the primary accession code PRJEB29654. The raw datasets will be made available through Dryad, a reporting summary will be provided. The analysed datasets that support our findings are available as supplementary datasets. The associated raw data for Figures 2 and 3 are provided in Supplementary data 1, the raw data for Table 1 are provided in Supplementary data 2. The germplasm generated in this project will be available via NASC.

Materials and Methods:

Plant materials

Seven Arabidopsis accessions were chosen for the construction of a full nucleotype-plasmotype diallel. Ely (CS28631) is atrazine resistant due to a chloroplast-encoded mutation in *PsbA* which leads to a modified D2 protein that greatly reduces PSII efficiency (El-Lithy et al., 2005). Ws-4 (CS5390) was included for its unusual photosystem II phosphorylation dynamics (Yin et al., 2012). Bur (CS76105) is commonly used in diversity panels and is a standard reference accession. Sha (CS76227) was selected based on its capacity to induce cytoplasmic male sterility in some crosses (Gobron et al., 2013). The set was completed by adding L*er* (CS76164), Col (CS76113) and C24 (CS76106) which are three widely used genotypes in Arabidopsis research. Col is the reference genome for nuclear and chloroplast sequences and C24 for the mitochondrial sequence. The *GFP-tailswap* haploid-inducer (Ravi and Chan, 2010) is in a Col background.

Generation of a nucleotype-plasmotype diallel

To generate new nucleotype-plasmotype combinations, plants of all seven accessions (Bur, C24, Col, Ely, L*er*, Sha and Ws-4) were crossed as males to *GFP-tailswap* (the Col plasmotype donor) as well as six newly generated haploid inducer lines (Fig. 1B). The haploids arising from these 49 crosses were identified based on their phenotype (as described in Wijnker et al. (2014)). These haploid lines were self-fertilized to obtain doubled haploid offspring (Fig. 1A). The resulting 49 lines comprise a full diallel of 21 pairs of reciprocal nucleotype-plasmotype combinations (cybrids) as well as seven nucleotype-plasmotype combinations that have the same nucleotype-plasmotype combinations as their wild-type progenitors (self-cybrids; Fig. 1B, diagonal). All cybrids and the wild-type accessions were propagated for one generation before use in further experiments, with the exception of Ely^{Sha} of which the original haploid died and had to be recreated thus limiting our analyses to 48 rather than 49 cybrids. Even though self-cybrids are genetically identical to their wild-type accessions, the parental lines were included in the screens to test for possible unforeseen effects of cybrid production (which involves a haploid growth stage). This brings the number of lines included in this study to a total of 55 (41 cybrids, 7 self-cybrids and 7 wild types).

Genotype confirmation

To confirm that all cybrids in our panel are authentic, all 49 cybrids and 7 wild-type progenitors were whole-genome sequenced at the Max Planck-Genome-centre Cologne (Germany) using Illumina Hiseq 2500 150-bp paired-end sequencing. The cybrids were sequenced at 8.5X coverage and the wild-type progenitors at 40X coverage. Reads were aligned against the TAIR10 reference sequence, including organellar sequences, followed by variant calling using SHORE and GenomeMapper (Ossowski et al., 2008; Schneeberger et al., 2009). For the nucleus we used a phred quality score of 40, leaving 92022 SNPs and for the chloroplast used a phred quality score of 15, leaving 289 SNPs. 46 cybrids were found to have the correct genotypes. With one line, $Bur^{Ws\text{-}4}$, there was a sample mix-up during library preparation with Sha^{Sha}. To confirm sequences we therefore used the Sha genotype (CS76382) from the 1001 genomes project (The 1001 Genomes Consortium, 2016). Two other lines, $C24^{C24}$ and $Ws\text{-}4^{Col}$, had a high number of heterozygous calls, which we attributed to sample contamination. To ensure that the sample mix-up and the putative event of cross-contamination occurred in the laboratory, we designed KASP™ makers (LGC, https://www.lgcgroup.com) and genotyped all lines. These KASP™ markers are chloroplast specific and were designed based on the obtained sequence data (Supplementary Table 7). All lines showed the correct genotypes, and no heterozygosity was observed in any of the lines, including $C24^{C24}$ and $Ws\text{-}4^{Col}$. In summary we confirmed that all 49 cybrids had the correct genotype. Unfortunately the Ely^{Sha} used for sequencing died before setting seed and although it has since been recreated, it could not be included in our phenotypic analyses.

Phenotyping

Cybrids were phenotypically assessed using different platforms. Growth, PSII efficiency, chlorophyll reflectance and leaf movement (all parameters at n=24) was screened in the Phenovator platform, a high-throughput phenotyping facility located in a climate-controlled growth chamber (Flood et al., 2016). This phenotyping platform measured the plants for: photosynthetic efficiency (φ_{PSII}) using chlorophyll fluorescence, reflectance at 480 nm, 532 nm, 550 nm, 570 nm, 660 nm, 700 nm, 750 nm and 790 nm, and projected leaf area (PLA) based on pixel counts of near infra-red (NIR) images (Flood et al., 2016). The growth chamber was set to a 10 h day/14 h night regime, at 20°C day and 18°C night temperature, 200 µmol m^{-2} s^{-1} irradiance, and 70% relative humidity. The plants were grown

on a rockwool substrate and irrigated daily with a nutrient solution as described in Flood et al. (2016). Growth (n=24) and subsequently above ground biomass (n=12) was measured in another high-throughput phenotyping facility (Kokorian et al., 2010), where projected leaf area was measured three times per day with 14 fixed cameras (uEye Camera, IDS Imaging Development Systems GmbH, Obersulm, Germany). This growth chamber was set to a 10 h day/14 h night regime, at 20°C day and 14°C night temperature, 200 µmol m^{-2} s^{-1} light and 70% relative humidity. Plants were grown on rockwool and irrigated weekly with a nutrient solution as described before. Non-fluctuating and fluctuating light treatments were performed in the DEPI phenotyping facility (n=4) (Cruz et al., 2016). This facility is able to measure the chlorophyll fluorescence derived photosynthetic parameters, φ_{PSII}, NPQ, q_E, q_I. Three week old plants were moved into the facility, where they were left to acclimatize for 24 hours after which three days of phenotyping was performed under different light regimes. On the first day the plants were illuminated with a constant light intensity of 200 µmol m^{-2} s^{-1}. On the second day the plants received a sinusoidal light treatment where the light intensity began low and gradually increased to a maximum of 500 µmol m^{-2} s^{-1} light from which it deceased back down to 0. On the third day the plants received a fluctuating light treatment ranging between 0 and 1000 µmol m^{-2} s^{-1} light in short intervals. For further details see Cruz et al. (2016). Bolting time and flowering time were measured on all cybrids (n=10) in a greenhouse experiment in April 2017, with the exception of Ely nucleotype cybrids which needed vernalisation and were not included in this experiment. Additional lighting was turned on when the natural light intensity fell below 685.5 µmol m^{-2} s^{-1}, and turned off when the light intensity reached 1142.5 µmol m^{-2} s^{-1}, with a maximum of 16 h per day.

Seeds for the germination experiments were stratified on wet filter paper for four days at 4°C before being assayed in the Germinator platform (Joosen et al., 2010) for seed size, germination rate and total germination percentage. All seeds were generated from two rounds of propagation. In the first round seeds were first sown in a growth chamber set to a 10 h day/14 h night regime, at 20°C day and 18°C night temperature. 200 µmol$m^{-2}s^{-1}$ light intensity, and 70% relative humidity. After three weeks they were moved to an illuminated cold room at 4°C for six weeks of vernalization. After vernalization all plants (n=8) were moved to a temperature-controlled greenhouse (20°C) for flowering and seed ripening. Exceptions to this were L*er*^{Ely}, L*er*$^{Ws\text{-}4}$, and Ely$^{Ws\text{-}4}$ for which no doubled haploid seed was available at the beginning of the first propagation round. L*er*^{Ely} and L*er*$^{Ws\text{-}4}$ were sown later, during the vernalization stage and flowered at the same time as the vernalized plants. Ely$^{Ws\text{-}4}$

produced haploid seed at a later stage and could not be included in the first propagation round. Plants were grown in a temperature-controlled greenhouse set at 20°C. In this round only lines with the Ely nucleotype were vernalized.

Metabolomics

Plant material for primary metabolite analysis was obtained from the 'Phenovator' photosynthetic phenotyping experiment. Plants were harvested 26 days after sowing, which due to the 10-hr photoperiod was prior to bolting for all lines. Samples were frozen in liquid nitrogen, and samples of each genotype were subsequently combined into four pools each made up of material of approximately six replicates. Each pool was ground and homogenized before an aliquot was taken for further analysis. Reference samples for the metabolite analysis were composed of material from all seven parents in equal amounts and then homogenized. The method used for the extraction of polar metabolites from Arabidopsis leaves was adapted from Lisec et al. (2006) as described by Carreno-Quintero et al. (2012). Specific adjustments for Arabidopsis samples were made as follows; the polar metabolite fractions were extracted from 100 mg of Arabidopsis leaf material (fresh weight, with max. 5% deviation). After the extraction procedure, 100 µL aliquots of the polar phase were dried by vacuum centrifugation for 16 hours. The derivatization was performed on-line similar as described by Lisec et al. (2006) and the derivatized samples were analyzed by a GC-ToF-MS system composed of an Optic 3 high-performance injector (ATAS^{TM}, GL Sciences, Eindhoven, The Netherlands) and an Agilent 6890 gas chromatograph (Agilent Technologies, Santa Clara, United States) coupled to a Pegasus III time-of-flight mass spectrometer (Leco Instruments, St. Joseph, United States). Two microliters of each sample were introduced in the injector at 70°C using 5% of the sample (split 20). The detector voltage was set to 1750 Volts. All samples were analyzed in random order in four separate batches. The systematic variation that inadvertently is introduced by working in batches, was removed upon analysis of covariance. In this model the batch number was used as a factor (four levels) and "run number within a batch" as a covariate since it is also expected that (some) variation will be introduced by the sample run order within each batch. For this the S2 method described by (Wehrens et al., 2016) was used to perform the least-squares regression. After quality control and removing metabolites with more than 20% missing data and a broad sense heritability (H^2) of less than

5%, we were left with data on 41 primary metabolites. Metabolites were identified based on the level of identification standard by the Metabolomics Standards Initiative (Sumner et al., 2007).

Transcriptome analysis

Using the same material as described in the metabolome analysis, total RNA was extracted from all nine reciprocal cybrids between accessions Bur, L*er* and Ely, with three replicates per genotype, totaling 27 plants. Library preparation was done with a selection on 3' polyadenylated tails to preferentially include nuclear mRNA. Read alignment was done using TopHat (Trapnell et al., 2009). Any chloroplast and mitochondrial genes remaining were excluded from further analysis. The raw counts were normalized and analyzed using the DeSeq2 package in R (Love et al., 2014). Genes for which the expression levels were significantly different between two cybrids were determined by comparing two genotypes using the contrast function of DeSeq2. P-values were determined using the Wald test, and p-values were adjusted using the Benjamini-Hochberg correction (α=0.05). GO enrichment analysis was done using default setting in g:profiler Compact Compare of Annotations (g:Cocoa). The complete set of detected genes in each cybrid was used as a statistical background in the analysis (Reimand et al., 2016).

Phenotypic data analysis

We used the self-cybrids as our baseline in phenotypic comparisons to control for any possible effects of cybrid creation. Raw data was directly analyzed except for time series data of growth and chlorophyll reflectance which was preprocessed as follows. Time series data were fitted with a smooth spline using the gam function from the mgcv package in R (Wood et al., 2016). The fitted B-spline was subsequently used to derive several curve parameters. In addition, we calculated relative growth rate per time point by dividing the growth rate, relative to the plant size (Flood et al., 2016). All raw parameters and derived parameters were analyzed by fitting either a linear mixed model or a linear model. The linear mixed model was used when a random correction parameter was present, when such random correction parameters were absent a linear model was used. The models were analyzed using the Restricted Maximum Likelihood (REML) procedure for each relevant trait using the lme4 package in R (Bates et al., 2015). As each experiment had a different design, several models were employed (Supplementary Table 4). The following model was generally used, in some instances random terms (underlined below) were added:

$$\underline{Y} = Nucleotype + Plasmotype + (Nucleotype * Plasmotype) + \underline{Block} + \underline{\varepsilon} \quad (1)$$

For every model, normality and equal variances were checked. Next for every phenotypic parameter it was determined whether an interaction model or a plasmotype additive model would suit best. This was done by ANOVA in which Kenward-Roger approximation for degrees of freedom was used. As posthoc tests we used Dunnett's test, where we tested (two sided) whether a given cybrid was different from the self-cybrid control. The significance threshold for the posthoc tests was set at α=0.05. The contribution of the nucleotype, plasmotype and the interaction between the two, was determined by estimating the variance components in mixed models containing the same terms as in model (1). However the fixed terms were taken as random:

$$\underline{Y} = \underline{Nucleotype} + \underline{Plasmotype} + \underline{(Nucleotype * Plasmotype)} + \underline{Block} + \underline{\varepsilon},$$

Where the variance components were estimated by the VarCorr function from the lme4 package. Total variance was calculated by summing all the variance components, after which the fraction explained variance for every term in the model was calculated. The broad sense heritability, in our case equal to repeatability (Falconer and Mackay, 1996), is determined by the three genetic components, i.e. nucleotype, plasmotype and the interaction, together. The fraction of broad sense heritability explained by the separate genetic components was calculated subsequently.

In total we measured 1008 phenotypes. However many were highly correlated, particularly in the time series data. After data processing, further analysis was only conducted on phenotypes with a broad sense heritability higher than 5%, removing phenotypes that were non-informative, leaving with 906 phenotypes. Furthermore, to avoid biases in the results due to overly correlated data, when stating summary statistics, we wanted to get a representative set of phenotypes from the remaining 906 phenotypes (Supplementary Table 1). Using a threshold based purely on correlation would favor the inclusion of variation largely driven by the nucleotype, thus we sought to include a subset of time points from each time series. We therefore selected the following representative phenotypes. For time series in which we scored for up to 25 days after germination, we selected mornings of day 8, 13, 18 and 23. The time series analysis of fluctuating light were only measured for three days in a row, with

each day a different treatment. As these treatments reached their extremes in the middle of the day, these time points were selected. For the different seed treatments we used the germination time until 50% of the seeds germinated. In addition we included biomass, leaf movement, seed size and flowering time as single phenotypes. All data on the 1008 phenotypes are available in Supplementary Data 1.

References:

Bates D, Mächler M, Bolker B, Walker S (2015) Fitting linear mixed-effects models using lme4. Journal of Statistical Software **67:** 48

Bock DG, Andrew RL, Rieseberg LH (2014) On the adaptive value of cytoplasmic genomes in plants. Molecular Ecolology **23:** 4899-4911

Carreno-Quintero N, Acharjee A, Maliepaard C, Bachem CWB, Mumm R, Bouwmeester H, Visser RGF, Keurentjes JJB (2012) Untargeted metabolic quantitative trait loci analyses reveal a relationship between primary metabolism and potato tuber quality. Plant Physiology **158:** 1306-1318

Chen X-Y, Kim J-Y (2009) Callose synthesis in higher plants. Plant Signaling & Behavior **4:** 489-492

Cruz JA, Savage LJ, Zegarac R, Hall CC, Satoh-Cruz M, Davis GA, Kovac WK, Chen J, Kramer DM (2016) Dynamic Environmental Photosynthetic Imaging Reveals Emergent Phenotypes. Cell Systems **2:** 365-377

Dobler R, Rogell B, Budar F, Dowling DK (2014) A meta-analysis of the strength and nature of cytoplasmic genetic effects. J. Evolution Biol. **27:** 2021-2034

El-Lithy ME, Rodrigues GC, van Rensen JJS, Snel JFH, Dassen HJHA, Koornneef M, Jansen MAK, Aarts MGM, Vreugdenhil D (2005) Altered photosynthetic performance of a natural Arabidopsis accession is associated with atrazine resistance. Journal of Experimental Botany **56:** 1625-1634

Falconer D, Mackay T (1996) Introduction to quatitative genetics (4th ed) Harlow, England: Longman

Flood PJ, Kruijer W, Schnabel SK, Schoor R, Jalink H, Snel JFH, Harbinson J, Aarts MGM (2016) Phenomics for photosynthesis, growth and reflectance in Arabidopsis thaliana reveals circadian and long-term fluctuations in heritability. Plant Methods **12:** 1-14

Flood PJ, van Heerwaarden J, Becker F, de Snoo CB, Harbinson J, Aarts MGM (2016) Whole-Genome Hitchhiking on an Organelle Mutation. Current Biology **26:** 1306-1311

Flood PJ, Yin L, Herdean A, Harbinson J, Aarts MGM, Spetea C (2014) Natural variation in phosphorylation of photosystem II proteins in Arabidopsis thaliana: is it caused by genetic variation in the STN kinases? Philosophical Transactions of the Royal Society B: Biological Sciences **369**

Forde BG, Roberts MR (2014) Glutamate receptor-like channels in plants: a role as amino acid sensors in plant defence? F1000Prime Reports **6:** 37

Gobron N, Waszczak C, Simon M, Hiard S, Boivin S, Charif D, Ducamp A, Wenes E, Budar F (2013) A Cryptic Cytoplasmic Male Sterility Unveils a Possible Gynodioecious Past for *Arabidopsis thaliana*. PLoS ONE **8:** e62450

Joosen RVL, Kodde J, Willems LAJ, Ligterink W, van der Plas LHW, Hilhorst HWM (2010) germinator: a software package for high-throughput scoring and curve fitting of Arabidopsis seed germination. The Plant Journal **62:** 148-159

Joseph B, Corwin JA, Li B, Atwell S, Kliebenstein DJ (2013) Cytoplasmic genetic variation and extensive cytonuclear interactions influence natural variation in the metabolome. eLife **2:** e00776

485 **Joseph B, Corwin JA, Züst T, Li B, Iravani M, Schaepman-Strub G, Turnbull LA, Kliebenstein DJ**
486 (2013) Hierarchical Nuclear and Cytoplasmic Genetic Architectures for Plant Growth and
487 Defense within Arabidopsis. The Plant Cell **25:** 1929-1945
488 **Kindiger B, Hamann S** (1993) Generation of Haploids in Maize: A Modification of the Indeterminate
489 Gametophyte (ig) System. Crop Science **33:** 342-344
490 **Kleine T, Leister D** (2016) Retrograde signaling: Organelles go networking. Biochimica et Biophysica
491 Acta (BBA) - Bioenergetics **1857:** 1313-1325
492 **Kokorian J, Polder G, Keurentjes JJB, Vreugdenhil D, Olortegui Guzman MC** (2010) An ImageJ
493 based measurement setup for automated phenotyping of plants. *In* A Jahnen, C Moll, eds,
494 Proceedings of the ImageJ User and Developer Conference, Luxembourg, Luxembourg, 27-
495 29 October 2010. Centre de Recherche Public Henri Tudor, Luxembourg, pp 178-182
496 **Kromdijk J, Głowacka K, Leonelli L, Gabilly ST, Iwai M, Niyogi KK, Long SP** (2016) Improving
497 photosynthesis and crop productivity by accelerating recovery from photoprotection. Science
498 **354:** 857-861
499 **Levings CS** (1990) The Texas Cytoplasm of Maize: Cytoplasmic Male Sterility and Disease
500 Susceptibility. Science **250:** 942-947
501 **Lisec J, Schauer N, Kopka J, Willmitzer L, Fernie AR** (2006) Gas chromatography mass
502 spectrometry-based metabolite profiling in plants. Nature Protocols **1:** 387-396
503 **Love MI, Huber W, Anders S** (2014) Moderated estimation of fold change and dispersion for RNA-
504 seq data with DESeq2. Genome Biology **15:** 550
505 **Lv F, Zhou J, Zeng L, Xing D** (2015) β-cyclocitral upregulates salicylic acid signalling to enhance
506 excess light acclimation in Arabidopsis. Journal of Experimental Botany **66:** 4719-4732
507 **Miclaus M, Balacescu O, Has I, Balacescu L, Has V, Suteu D, Neuenschwander S, Keller I,**
508 **Bruggmann R** (2016) Maize Cytolines Unmask Key Nuclear Genes That Are under the
509 Control of Retrograde Signaling Pathways in Plants. Genome Biology and Evolution **8:** 3256-
510 3270
511 **Nguyen CT, Kurenda A, Stolz S, Chételat A, Farmer EE** (2018) Identification of cell populations
512 necessary for leaf-to-leaf electrical signaling in a wounded plant. Proceedings of the National
513 Academy of Sciences **115**:10178-10183.
514 **Ossowski S, Schneeberger K, Clark RM, Lanz C, Warthmann N, Weigel D** (2008) Sequencing of
515 natural strains of Arabidopsis thaliana with short reads. Genome Research **18:** 2024-2033
516 **Ravi M, Chan SWL** (2010) Haploid plants produced by centromere-mediated genome elimination.
517 Nature **464:** 615-618
518 **Ravi M, Marimuthu MPA, Tan EH, Maheshwari S, Henry IM, Marin-Rodriguez B, Urtecho G, Tan**
519 **J, Thornhill K, Zhu F, Panoli A, Sundaresan V, Britt AB, Comai L, Chan SWL** (2014) A
520 haploid genetics toolbox for Arabidopsis thaliana. Nature Communications **5:** Article number:
521 5334
522 **Reimand J, Arak T, Adler P, Kolberg L, Reisberg S, Peterson H, Vilo J** (2016) g:Profiler—a web
523 server for functional interpretation of gene lists (2016 update). Nucleic Acids Research **44:**
524 W83-W89
525 **Roux F, Mary-Huard T, Barillot E, Wenes E, Botran L, Durand S, Villoutreix R, Martin-Magniette**
526 **M-L, Camilleri C, Budar F** (2016) Cytonuclear interactions affect adaptive traits of the annual
527 plant *Arabidopsis thaliana* in the field. Proceedings of the National Academy of Sciences **113:**
528 3687-3692
529 **Schneeberger K, Ossowski S, Lanz C, Juul T, Petersen AH, Nielsen KL, Jørgensen J-E, Weigel**
530 **D, Andersen SU** (2009) SHOREmap: simultaneous mapping and mutation identification by
531 deep sequencing. Nature Methods **6:** 550–551
532 **Somerville CR, Ogren WL** (1980) Photorespiration mutants of *Arabidopsis thaliana* deficient in
533 serine-glyoxylate aminotransferase activity. Proceedings of the National Academy of Sciences
534 **77:** 2684-2687
535 **Sumner LW, Amberg A, Barrett D, Beale MH, Beger R, Daykin CA, Fan TW-M, Fiehn O,**
536 **Goodacre R, Griffin JL, Hankemeier T, Hardy N, Harnly J, Higashi R, Kopka J, Lane AN,**

Lindon JC, Marriott P, Nicholls AW, Reily MD, Thaden JJ, Viant MR (2007) Proposed minimum reporting standards for chemical analysis. Metabolomics **3:** 211-221

Tang Z, Hu W, Huang J, Lu X, Yang Z, Lei S, Zhang Y, Xu C (2014) Potential Involvement of Maternal Cytoplasm in the Regulation of Flowering Time via Interaction with Nuclear Genes in Maize. Crop Science **54:** 544-553

The 1001 Genomes Consortium (2016) 1,135 Genomes Reveal the Global Pattern of Polymorphism in Arabidopsis thaliana. Cell **166:** 481-491

Toyota M, Spencer D, Sawai-Toyota S, Jiaqi W, Zhang T, Koo AJ, Howe GA, Gilroy S (2018) Glutamate triggers long-distance, calcium-based plant defense signaling. Science **361:** 1112-1115

Trapnell C, Pachter L, Salzberg SL (2009) TopHat: discovering splice junctions with RNA-Seq. Bioinformatics **25:** 1105-1111

Wehrens R, Hageman JA, van Eeuwijk F, Kooke R, Flood PJ, Wijnker E, Keurentjes JJB, Lommen A, van Eekelen HDLM, Hall RD, Mumm R, de Vos RCH (2016) Improved batch correction in untargeted MS-based metabolomics. Metabolomics **12:** 88

Wijnker E, Deurhof L, van de Belt J, de Snoo CB, Blankestijn H, Becker F, Ravi M, Chan SWL, van Dun K, Lelivelt CLC, de Jong H, Dirks R, Keurentjes JJB (2014) Hybrid recreation by reverse breeding in Arabidopsis thaliana. Nature Protocols **9:** 761-772

Wood SN, Pya N, Säfken B (2016) Smoothing Parameter and Model Selection for General Smooth Models. Journal of the American Statistical Association **111:** 1548-1563

Yin L, Fristedt R, Herdean A, Solymosi K, Bertrand M, Andersson MX, Mamedov F, Vener AV, Schoefs B, Spetea C (2012) Photosystem II Function and Dynamics in Three Widely Used *Arabidopsis thaliana* Accessions. PLoS ONE **7:** e46206

Zavaliev R, Levy A, Gera A, Epel BL (2013) Subcellular Dynamics and Role of Arabidopsis β-1,3-Glucanases in Cell-to-Cell Movement of Tobamoviruses. Molecular Plant-Microbe Interactions **26:** 1016-1030